Article

Discovery Medicine 2026; 38(210): 2164–2177
https://doi.org/10.24976/Discov.Med.202638210.169

Spatial Expression Patterns of the RANKL/RANK Axis and Inflammatory Markers in Remodeling-Associated Periodontal Tissues

Weilong Lin[1], Chao Li[1], Jinping Xiao[1], Jia Zhang[2], Xiaopei Wu[2,*]

[1]Department of Stomatology, First Hospital Affiliated to Hebei North University, 075000 Zhangjiakou, Hebei, China
[2]Department of Stomatology, Peking University Third Hospital Chongli, 075000 Zhangjiakou, Hebei, China
*Correspondence: wxpandlwl2617@163.com (Xiaopei Wu)
Submitted: 17 April 2026 Revised: 28 May 2026 Accepted: 22 June 2026 Published: 23 July 2026

Background: The remodeling of alveolar bone is governed by the Receptor Activator of Nuclear Factor Kappa-B Ligand (RANKL)/RANK/Osteoprotegerin (OPG) signaling axis, which is tightly regulated by the local immune microenvironment. However, previous studies utilizing whole-tissue homogenates have been unable to determine whether these molecular changes are spatially restricted to specific remodeling niches. This study aimed to characterize the site-specific molecular signature of the RANKL pathway and its association with inflammatory cytokines in periodontal tissues.

Methods: A rat model of orthodontic tooth movement (OTM) was established. Laser Capture Microdissection (LCM) was employed to precisely isolate remodeling-associated periodontal tissues and physiological baseline tissues. mRNA expression of *RANKL*, *RANK*, *OPG*, and Nuclear Factor of Activated T-cells, cytoplasmic 1 (*NFATc1*) in these micro-dissected regions was quantified using qPCR. Whole-tissue lysates were analyzed by Western blotting for inflammatory cytokines (Tumor Necrosis Factor-alpha (TNF-α), interleukin (IL)-1β, IL-6). *In vitro*, human periodontal ligament cells (hPDLCs) were stimulated with TNF-α to investigate whether inflammatory stimulation is accompanied by changes in osteoclast-related molecular markers.

Results: Histological and tartrate-resistant acid phosphatase (TRAP) staining indicated increased osteoclast-rich remodeling activity in selected regions. LCM-based analysis revealed spatially restricted upregulation of *RANKL*, *RANK*, and *NFATc1*, coupled with a disrupted *RANKL/OPG* ratio specifically within remodeling microenvironments, distinct from the surrounding tissue. Whole-tissue Western blotting showed concomitant increases in inflammatory cytokines and osteoclast-related proteins at the tissue level. TNF-α stimulation of hPDLCs increased the *RANKL/OPG* ratio and Macrophage Colony-Stimulating Factor (*M-CSF*) expression, suggesting that inflammatory stimulation may promote a molecular state permissive for osteoclast-related signaling.

Conclusion: LCM-based analysis revealed that disruption of the local RANKL/OPG balance and upregulation of osteoclast-related molecules are spatially restricted to remodeling microenvironments rather than uniformly distributed across periodontal tissues. *In vitro*, TNF-α stimulation of hPDLCs dose-dependently shifted the molecular profile toward a state permissive for osteoclast-related signaling. These findings underscore the importance of spatial resolution in periodontal remodeling research and support a potential link between local inflammatory cues and altered osteoclast-related molecular signaling.

Keywords: orthodontic tooth movement; periodontal remodeling; RANKL/RANK signaling; laser capture microdissection; TNF-α; spatial heterogeneity

Introduction

The structural integrity of the periodontium is maintained through a dynamic equilibrium of alveolar bone remodeling, a process that requires the stringent coordination of bone formation by osteoblasts and resorption by osteoclasts [1,2]. Under physiological conditions, this metabolic turnover is homeostatically regulated; however, pathological stimuli, such as chronic inflammation in periodontitis or mechanical stress during orthodontic tooth movement, often disrupt this balance, precipitating net bone loss [3,4]. Central to this pathological shift is the aberrant recruitment and activation of osteoclasts, multinucleated giant cells derived from the monocyte-macrophage lineage [5]. While the cellular machinery of resorption is well-characterized, the precise molecular interplay within the periodontal microenvironment that initiates this cascade remains a critical area of inquiry.

The molecular regulation of osteoclastogenesis is primarily governed by the Receptor Activator of Nuclear Factor Kappa-B Ligand (RANKL) signaling axis [6]. RANKL, expressed by osteoblasts and periodontal ligament (PDL) fibroblasts, binds to its receptor RANK on osteoclast precursors, triggering a signaling trajectory that culminates in the induction of Nuclear Factor of Activated T-cells, cytoplasmic 1 (NFATc1) [7,8]. NFATc1 serves as the master tran-

scriptional switch, integrating upstream signals to drive the expression of osteoclast-specific genes essential for fusion and function [9,10]. Critically, this process is restrained by Osteoprotegerin (OPG), a soluble decoy receptor that sequesters RANKL, preventing receptor engagement [11,12]. Thus, the local RANKL/OPG ratio, rather than the absolute level of either molecule, acts as the definitive determinant of bone fate [13,14]. Additionally, Macrophage Colony-Stimulating Factor (M-CSF) plays an indispensable role by promoting the survival and proliferation of osteoclast precursors, thereby priming them for RANKL-induced differentiation [15,16].

This regulatory network does not operate in isolation but is intimately entwined with the immune system, a cross-disciplinary field termed "osteoimmunology" [17]. Inflammatory cytokines, particularly Tumor Necrosis Factor-alpha (TNF-α), Interleukin-1 beta (IL-1β), and IL-6, function as potent modulators of this system [18,19]. These cytokines can directly enhance RANKL expression in stromal cells or synergize with RANK signaling to amplify downstream effector pathways [20]. In the context of the periodontium, PDL cells are uniquely positioned to sense these inflammatory cues and translate them into osteoclastogenic signals [21,22]. However, the heterogeneity of the periodontal landscape means that inflammation and remodeling are often spatially restricted phenomena.

Precisely how these inflammatory signals converge with the RANKL/RANK axis within defined remodeling microenvironments, rather than across the tissue as a whole, therefore remains a key unresolved question.

Despite extensive evidence implicating the RANKL/RANK axis and inflammatory cytokines in periodontal remodeling, the spatial resolution of existing studies is significantly limited. The majority of previous investigations have relied on whole-tissue homogenates, which inherently obscure the molecular heterogeneity across distinct microenvironments within the periodontium. Although laser capture microdissection (LCM) has previously been applied to periodontal and orthodontic tissues, including studies examining heat shock protein gene expression in the pressure zone of the PDL during early tooth movement [23] and proteomic profiling of the PDL under orthodontic force [24], these investigations were not designed to address the spatial heterogeneity of the RANKL/OPG axis between morphologically distinct remodeling and quiescent regions. Critically, whether the RANKL/OPG imbalance and osteoclast-related molecular activation are spatially restricted phenomena confined to active remodeling microenvironments, or represent diffuse changes uniformly distributed across the periodontal tissue, has not been directly addressed. To address this gap, we used laser capture microdissection to directly compare morphologically defined remodeling-associated and quiescent periodontal regions within the same orthodontic tooth movement (OTM) specimens, thereby determining whether osteoclast-related molecular alterations are spatially restricted rather than diffusely distributed throughout periodontal tissues.

Materials and Methods

Experimental Model and Tissue Collection

Periodontal tissues were obtained from a rat model of (OTM, n = 6 rats). 12 male Sprague-Dawley rats (8 weeks old, 200–250 g; Vital River, Beijing, China) were used. Under general anesthesia with pentobarbital sodium (50 mg/kg, i.p.; P1081, Beyotime, Shanghai, China), a nickel-titanium closed-coil spring was ligated between the maxillary first molar and the ipsilateral incisors to deliver a continuous mesial force of 50 g, calibrated with a tension gauge, for 7 days. The appliance was inspected every other day and reactivated if loosened. Rats were housed under standard conditions (12-h light/dark cycle, 22 ± 2 ℃) with soft chow and water *ad libitum*. For LCM-based analyses, tartrate-resistant acid phosphatase (TRAP) staining, and immunohistochemistry, the periodontal tissues of the OTM-loaded maxillary first molar were used, with Remodeling-associated and Reference regions sampled from the same tissue section of the same tooth (see ROI definition below). For whole-tissue Western blot analysis, in which the protein yield obtainable by LCM is insufficient, the contralateral unloaded maxillary first molar of the same animal was used as the internal control. After being anesthetized with pentobarbital sodium (50 mg/kg, i.p.; P1081, Beyotime, Shanghai, China) and sacrificed by decapitation, maxillary specimens were harvested and immediately fixed in 4% paraformaldehyde (Sigma-Aldrich, St. Louis, MO, USA). Samples were decalcified in ethylenediaminetetraacetic acid (EDTA; E9884, Sigma-Aldrich, St. Louis, MO, USA), processed, and embedded in paraffin for subsequent histological and molecular analyses. All animal experiments were approved by the Institutional Animal Care and Use Committee of Hebei North University, under protocol number HBNU20251112169, and were conducted in accordance with the ARRIVE Guidelines 2.0.

To precisely investigate the molecular signature of local microenvironments, LCM was employed. Maxillary specimens were fixed, decalcified, and embedded in paraffin. Serial sections (thickness 4 μm) were mounted on PEN (polyethylene naphthalate) membrane slides (11505158, Leica Microsystems, Wetzlar, Germany).

Sections were stained with Hematoxylin/Eosin for morphological identification. Two distinct Regions of Interest (ROIs) were defined and dissected using an LCM system (Leica LMD7, Leica Microsystems, Wetzlar, Germany), and ROI selection was performed according to predefined histomorphologic criteria to minimize subjective bias:

1. Remodeling-associated ROIs: Areas adjacent to resorption lacunae with high cellularity and multinucleated cells.

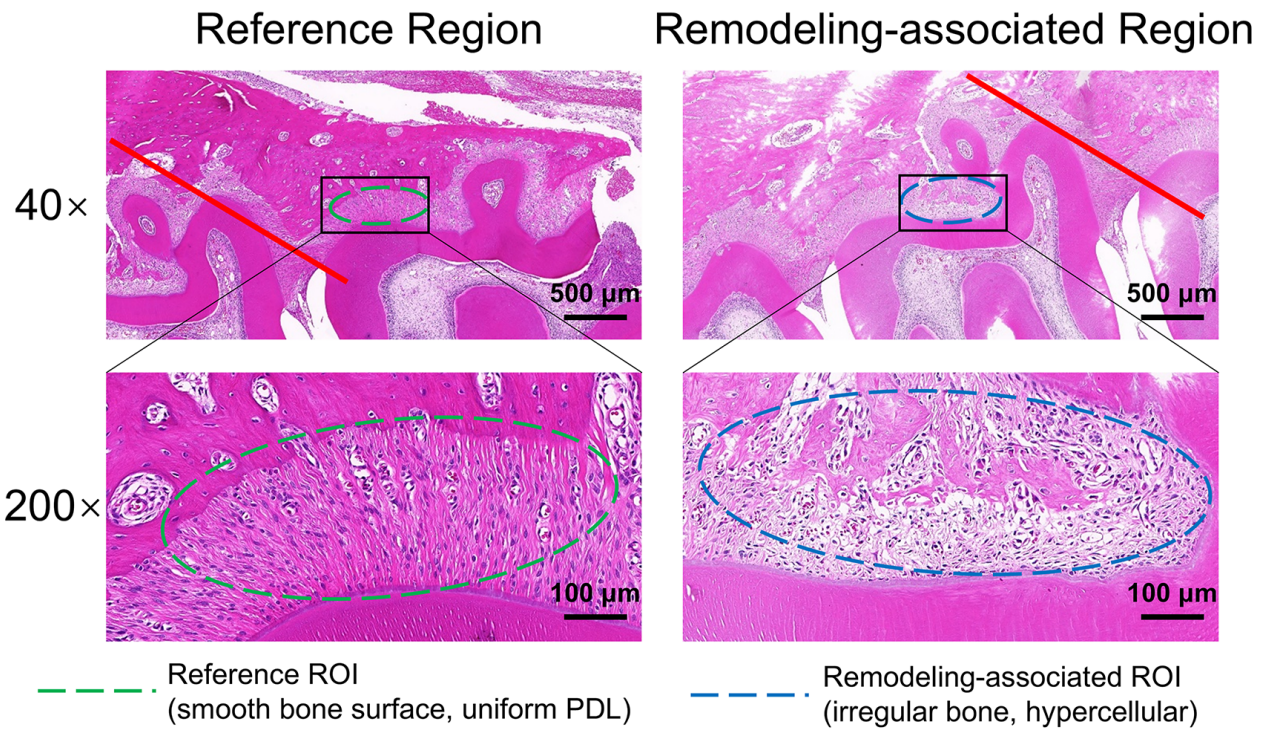

Fig. 1. Histological features of periodontal tissues. Representative hematoxylin and eosin (HE) stained sections of periodontal tissues at 40× and 200× magnification. Green dashed outlines indicate representative Reference ROIs, defined as areas adjacent to smooth alveolar bone surfaces with uniform periodontal ligament (PDL) width. Blue dashed outlines indicate representative Remodeling-associated ROIs, defined as areas adjacent to irregular bone surfaces with increased cellularity, indicative of active bone remodeling. The solid red line in each 40× panel demarcates the boundary between the Remodeling-associated area and the adjacent Reference region, as defined by the morphologic criteria. Scale bars are shown in each panel. ROIs, Regions of Interest.

2. Physiological Baseline ROIs: Areas adjacent to smooth bone surfaces with uniform PDL width.

Representative examples of these two ROI categories are demarcated in Fig. 1 (green dashed outlines, Reference ROIs; blue dashed outlines, Remodeling-associated ROIs).

Histological Analysis

Paraffin-embedded periodontal tissue samples were sectioned at a thickness of 4–5 µm. Sections were deparaffinized, rehydrated, and stained with hematoxylin and eosin (HE) following standard protocols. Histological evaluation was performed under light microscopy (Nikon Eclipse E100, Nikon Corporation, Tokyo, Japan) to assess periodontal ligament architecture and alveolar bone morphology. For ROI identification and morphological reference, representative HE-stained sections were selected independently and were not intended as serially matched sections for comparison with TRAP or immunohistochemical staining.

Identification and Quantification of Osteoclasts (TRAP Staining)

TRAP staining was performed on paraffin sections to identify osteoclasts using the TRAP Staining Kit (G1050-50T, Servicebio, Wuhan, China). TRAP-positive multinucleated cells located along alveolar bone surfaces were considered osteoclasts.

Quantitative analysis was conducted by counting the number of TRAP-positive cells per microscopic field in reference tissues and remodeling-associated tissues. For each sample, multiple non-overlapping fields were analyzed, and the average value was used for statistical analysis. Cell counting was performed in a blinded manner. For quantification, the number of TRAP-positive multinucleated cells (≥3 nuclei) was counted in 3 non-overlapping high-magnification fields per section per animal, and the mean count per animal was used as a single biological replicate. Statistical analysis was performed on per-animal values (n = 6 animals per group).

RNA Extraction and Quantitative Real-Time PCR Analysis

Total RNA was extracted from the micro-dissected tissue fragments using the Arcturus PicoPure RNA Isolation Kit (KIT0204, Applied Biosystems, Thermo Fisher Scientific, Waltham, MA, USA), optimized for FFPE (Formalin-Fixed Paraffin-Embedded) samples. Briefly, the captured tissues were incubated in extraction buffer at 42 ℃ for 30 minutes and then centrifuged. Total RNA was reverse-transcribed into cDNA using a First Strand cDNA Synthesis Kit (D7180M, Beyotime, Shanghai, China) according to the manufacturer's instructions. Quantitative real-time PCR was performed with a SYBR Green master mix (D7601S, Beyotime, Shanghai, China) on the LightCycler 96 PCR system (Roche, Mannheim, Germany). Each 20-µL reaction contained cDNA template, gene-specific primers, and SYBR Green master mix. Cycling conditions were 95 ℃ for 30 s, followed by 40 cycles of 95 ℃ for 5 s and 60 ℃ for 30 s, with a final melt-curve analysis to confirm amplification specificity. All samples were run in triplicate, and gene expression was normalized to glyceraldehyde-3-phosphate dehydrogenase (GAPDH). Gene expression in Remodeling ROIs was normalized to GAPDH and expressed relative to Baseline ROIs.

Quantitative real-time PCR was performed to evaluate the mRNA expression levels of RANKL (TNFSF11), RANK (TNFRSF11A), OPG (TNFRSF11B), NFATc1, and acid phosphatase 5 (ACP5). Gene expression levels were normalized to an internal control gene and expressed relative to the reference tissues using the $2^{-\Delta\Delta Ct}$ method. The RANKL/OPG mRNA ratio was calculated by dividing the relative expression level ($2^{-\Delta\Delta Ct}$) of RANKL by that of OPG for each sample, with the control group set to 1. Primer sequences are shown in Table 1.

Table 1. Primer sequences used in *in vivo* experiments.

Primer name	Primer Sequences (5′-3′)
RANKL	F: CCGAGACTACGGCAAGTACC
	R: ATCCATGCTAAGGCTCCACA
RANK	F: CTCCTCCCATTGCAGGTGAC
	R: AGGAGCAGGACGATGAGACT
OPG	F: CTGGAACCCCAGAGCGAAAT
	R: GCGTTTACTTTGGTGCCAGG
NFATc1	F: TCAGAGTGAGACCGAGAGGC
	R: AAGGAACAGCTGAGATGCCC
ACP5	F: TCTCTTCTACTGAGAGGTGCGA
	R: GAGTGGGAGCAGCAGGATTT
GAPDH	F: GTGGATATTGTTGCCATCAATGACC
	R: GCCCCAGCCTTCTTCATGGTGGT

RANKL, Receptor Activator of Nuclear Factor Kappa-B Ligand; OPG, Osteoprotegerin; NFATc1, Nuclear Factor of Activated T-cells, cytoplasmic 1; ACP5, acid phosphatase 5; GAPDH, glyceraldehyde-3-phosphate dehydrogenase; R, reverse; F, forward.

Protein Extraction and Western Blot Analysis

Because the protein yield obtainable by LCM is insufficient for Western blot analysis, whole periodontal tissues were harvested separately for protein analysis. Specifically, the OTM-loaded maxillary first molar served as the remodeling-associated tissue, and the contralateral unloaded first molar of the same animal served as the reference tissue. Freshly dissected, non-fixed periodontal tissues were used, separate from the formalin-fixed, decalcified, paraffin-embedded specimens. Immediately after sacrifice, periodontal tissues surrounding the OTM-loaded maxillary first molar and its contralateral unloaded counterpart were rapidly dissected from the alveolar bone under a stereomicroscope on ice, snap-frozen in liquid nitrogen, and stored at –80 ℃ until further analysis. For each sample, frozen tissues were pulverized in liquid nitrogen using a pre-chilled mortar and pestle, and the resulting powder was homogenized in ice-cold RIPA lysis buffer (P0013, Beyotime, Shanghai, China) supplemented with 1 mM PMSF and a phosphatase inhibitor cocktail at a ratio of approximately 1:10 (w/v). Homogenates were incubated on ice for 30 min with intermittent vortexing, then centrifuged at 12,000 ×g for 15 min at 4 ℃. Supernatants were collected, and total protein concentration was determined using a bicinchoninic acid (BCA) Protein Assay Kit (23225, Thermo Scientific, Shanghai, China).

Equal amounts of protein (~30 µg per lane) were separated by sodium dodecyl sulfate-polyacrylamide gel electrophoresis (SDS-PAGE) on 10% or 12% gels and transferred to polyvinylidene fluoride (PVDF) membranes (IPVH00010, Bedford, MA, USA). Membranes were blocked with 5% non-fat milk in Tris-buffered saline with Tween-20 (TBST) for 1 h at room temperature and then incubated (1:1000) overnight at 4 ℃ with primary antibodies against RANKL (HA500369, HUABIO, Hangzhou, China), RANK (ER1915-70, HUABIO, Hangzhou, China), NFATc1 (66963-1-Ig, Proteintech, Wuhan, China), IL-1β (HA723965, HUABIO), TNF-α (60291-1-Ig, Proteintech), and IL-6 (EM1701-45, HUABIO), and GAPDH (TA-08, ZSGB, Beijing, China). After three washes with TBST, membranes were incubated (1:5000) with HRP-conjugated secondary antibodies (SA00001-2/SA00001-1, Proteintech) for 1 h at room temperature. Protein bands were visualized using enhanced chemiluminescence (Millipore, Billerica, MA, USA) and quantified by densitometric analysis using ImageJ (version 1.54b, National Institutes of Health, Bethesda, MD, USA). Protein expression levels were normalized to GAPDH and expressed relative to reference tissues.

Immunohistochemical Analysis

Immunohistochemical staining was performed on paraffin-embedded sections using antibodies against

RANKL (bs-0747R, Bioss) and RANK (bsm-63879R, Bioss, Beijing, China). Paraffin-embedded sections (4 μm) were deparaffinized and rehydrated. Heat-induced antigen retrieval was performed in EDTA buffer (pH 9.0). Endogenous peroxidase activity was quenched with 3% hydrogen peroxide for 10 min, and nonspecific binding was blocked with 5% BSA for 30 min at room temperature. Sections were then incubated overnight at 4 ℃ with primary antibodies. After washing, sections were incubated with an HRP-conjugated antibody (AF5006, Beyotime, Shanghai, China) and visualized with diaminobenzidine (DAB) substrate (ZLI-9017, ZSGB-BIO, Beijing, China), followed by hematoxylin counterstaining, dehydration, and mounting. Negative controls were prepared by omitting the primary antibody.

Immunoreactivity was evaluated in reference tissues and remodeling-associated tissues. Semi-quantitative analysis was performed by measuring integrated optical density (IOD) per unit area using image analysis software. Mean values from multiple fields were used for statistical analysis.

For histological comparison across staining modalities, adjacent serial paraffin sections from the same specimen and comparable anatomical level were used for TRAP and immunohistochemical staining. This allowed regional comparison of TRAP-positive osteoclast distribution and RANKL/RANK immunoreactivity in anatomically corresponding periodontal regions. Representative images shown in Figs. 2,5 were selected from adjacent serial sections of the same periodontal region whenever regional comparisons were performed.

Cell Culture and Inflammatory Stimulation

To explore whether these *in vivo* inflammatory signals could directly modulate osteoclast-related molecular markers in periodontal stromal cells, we performed *in vitro* experiments. Human periodontal ligament cells (hPDLCs; also designated human periodontal ligament fibroblasts, HPLF) were obtained from ScienCell Research Laboratories (2630; Carlsbad, CA, USA) and cultured in Dulbecco's modified Eagle's medium (DMEM; Thermo Fisher Scientific, Waltham, MA, USA) supplemented with 10% fetal bovine serum (FBS) and 1% penicillin/streptomycin at 37 ℃ in a humidified atmosphere containing 5% CO_2. The cells were authenticated using Short Tandem Repeat (STR) analysis and confirmed to be free of mycoplasma. Cells from passages 3–5 were used for experiments.

To mimic the inflammatory microenvironment *in vitro*, hPDLCs were seeded in 6-well plates at a density of 1×10^5 cells/well. Upon reaching 80% confluence, cells were serum-starved for 12 hours and then stimulated with recombinant human tumor necrosis factor-alpha (rhTNF-α; 300-01A, PeproTech, Cranbury, NJ, USA) at graded concentrations (0, 10, and 50 ng/mL) for 24 hours [25,26,27]. Cells cultured in medium without rhTNF-α served as the control group. TNF-α was selected as a representative inflammatory stimulus to provide a proof-of-principle test of whether inflammatory cues can shift hPDLCs toward an osteoclast-supportive molecular profile.

Gene Expression Analysis (In Vitro)

Total RNA was extracted from the cultured cells using the TRIzol reagent (15596026, Thermo Fisher Scientific, Carlsbad, CA, USA). Quantitative real-time PCR was performed as described in the previous section. The primer sequences used in the *in vitro* experiment are shown in Table 2. Relative mRNA expression levels were calculated using the $2^{-\Delta\Delta Ct}$ method. The RANKL/OPG ratio was determined to evaluate the osteoclastogenic potential of the hPDLCs and calculated by dividing the relative expression level ($2^{-\Delta\Delta Ct}$) of RANKL by that of OPG for each sample, with the control group set to 1.

Statistical Analysis

Data are presented as mean ± standard deviation (SD). Normality of data distribution was confirmed using the Shapiro-Wilk test, and homogeneity of variance was confirmed using Levene's test. Statistical comparisons between two groups were performed using paired Student's *t*-tests. For experiments involving multiple groups, data were analyzed using one-way analysis of variance (ANOVA) followed by Tukey's post hoc test for multiple comparisons. A value of $p < 0.05$ was considered statistically significant. All statistical analyses were performed using GraphPad Prism (version 8.0.2, GraphPad Software, Boston, MA, USA). Throughout this study, "n" denotes the number of biological replicates, independent animals for the *in vivo* experiments and independent experiments for the *in vitro* experiments. For cell-counting analyses, multiple non-overlapping fields per section were averaged to yield a single value per animal.

Results

Histological Features of Periodontal Tissues Revealed Regions Enriched With Bone Remodeling Activity

Histological examination of periodontal tissue sections revealed well-organized periodontal ligament architecture and adjacent alveolar bone surfaces (Fig. 1). In selected areas, morphological features suggestive of active remodeling were observed, including irregular bone surfaces and increased cellularity along the alveolar bone interface. These features were used as morphologic criteria for identifying remodeling-associated regions and defining ROIs for LCM analysis.

Table 2. Primer sequences used in the *in vitro* experiment.

Primer name	Primer sequences (5′-3′)
Human RANKL (TNFSF11)	F: TGATTCATGTAGGAGAATTAAACAGG R: GATGTGCTGTGATCCAACGA
Human OPG (TNFRSF11B)	F: GAACCCCAGAGTGAAATACAG R: CCTGAAGAATGCCTCCTCAC
Human IL-6	F: ACTCACCTCTTCAGAACGAATTG R: CCATCTTTGGAAGGTTCAGGTTG
Human M-CSF (CSF1)	F: GCTGTTGTTGGTCTGTCTC R: CATGCTCTTCATAATCCTTG
Human GAPDH	F: ACAACTTTGGTATCGTGGAAGG R: GCCATCACGCCACAGTTTC

OPG, Osteoprotegerin; IL-6, Interleukin-6; M-CSF, Macrophage Colony-Stimulating Factor.

Increased TRAP-Positive Osteoclasts Were Observed in Remodeling-Associated Periodontal Tissues

TRAP staining identified multinucleated TRAP-positive osteoclasts predominantly localized along alveolar bone surfaces. Quantitative analysis demonstrated a significantly increased number of TRAP-positive cells in bone remodeling-associated tissues compared with reference tissues ($p < 0.001$), indicating increased osteoclast abundance in remodeling-associated periodontal tissues (Fig. 2A,B). In anatomically corresponding regions of adjacent serial sections, these TRAP-enriched areas were compared with the RANKL/RANK immunohistochemical findings shown in Fig. 5.

Altered Expression of RANKL/RANK-Related Molecules in Remodeling-Associated ROIs

Quantitative real-time PCR analysis of laser-microdissected tissues demonstrated that RANKL and RANK mRNA expression levels were markedly elevated in remodeling-associated ROIs compared with baseline ROIs (Fig. 3). In contrast, the increase in OPG expression was less pronounced than that of RANKL, resulting in a significantly elevated RANKL/OPG ratio ($p < 0.001$). Consistently, expression of NFATc1 and ACP5 was upregulated ($p < 0.001$), consistent with increased osteoclast-related molecular activity in remodeling-associated ROIs.

Inflammatory Cytokines and Osteoclast-Related Proteins Were Concomitantly Elevated in Periodontal Tissue Homogenates

Western blot analysis of whole periodontal tissue homogenates revealed elevated protein levels of the inflammatory cytokines IL-1β, TNF-α, and IL-6, together with increased expression of RANKL, RANK, and NFATc1, in remodeling-associated tissues compared with reference tissues (Fig. 4A,B; $p < 0.001$). Because protein was extracted from whole-tissue lysates, these findings reflect the overall molecular status at the tissue level and are consistent with the LCM-based mRNA data. These whole-tissue protein data were included to characterize the overall inflammatory and osteoclast-related molecular context of the periodontal tissues and were not intended to provide spatially resolved evidence.

RANKL and RANK Immunoreactivity was Observed in Anatomically Corresponding Regions of Adjacent Serial Sections With Increased TRAP-Positive Osteoclasts

Immunohistochemical analysis showed that RANKL and RANK immunoreactivity was predominantly observed in periodontal ligament cells and along alveolar bone surfaces (Fig. 5A–C). In adjacent serial sections from anatomically corresponding periodontal regions, stronger RANKL/RANK immunoreactivity was observed in regions corresponding to TRAP-positive osteoclast-enriched areas shown in Fig. 2. These findings support a spatial correspondence between RANKL/RANK immunoreactivity and osteoclast-rich remodeling sites in anatomically matched serial sections, but do not establish direct cellular colocalization or cell-type specificity.

TNF-α Stimulation Altered the Expression of Osteoclast-Related and Inflammatory Markers in hPDLCs

Treatment with TNF-α significantly altered the expression profile of hPDLCs in a dose-dependent manner. As shown in Fig. 6, TNF-α stimulation markedly upregulated *RANKL* mRNA expression compared with the control group ($p < 0.001$), whereas *OPG* mRNA expression showed a decreasing trend ($p < 0.01$). Consequently, the *RANKL/OPG* ratio was significantly increased in the TNF-α-treated groups ($p < 0.001$). TNF-α stimulation also induced increased *IL-6* and *M-CSF* expression ($p < 0.001$). These findings suggest that inflammatory stimulation may shift hPDLCs toward a molecular profile associated with osteoclast-related signaling.

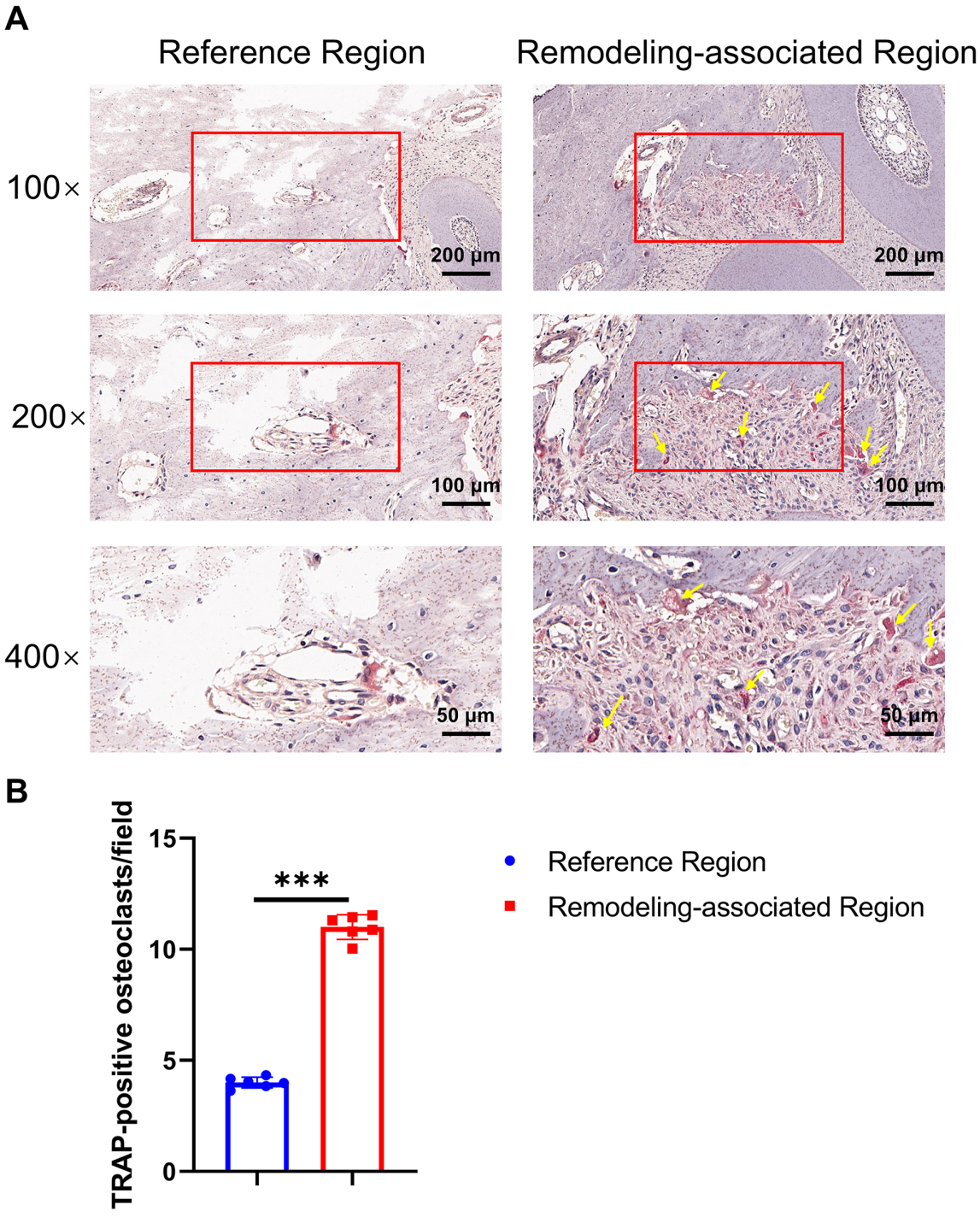

Fig. 2. Identification and quantification of osteoclasts in periodontal tissues by TRAP staining. (A) Representative TRAP-stained sections of periodontal tissues from the Reference Region (left column) and the Remodeling-associated Region (right column), shown at 100×, 200×, and 400× magnification. Yellow arrows on the 200× and 400× panels indicate representative multinucleated TRAP-positive osteoclasts, identified as large cells with red cytoplasmic TRAP signal and multiple nuclei located along the alveolar bone surface. In the Reference Region, no comparable multinucleated TRAP-positive osteoclasts were observed, and open spaces within the periodontal tissue correspond to physiological periodontal ligament and vascular/marrow spaces rather than sectioning artifacts. (B) Quantitative analysis of TRAP-positive osteoclast numbers per field in reference tissues and bone remodeling-associated tissues. Data are presented as mean ± SD (n = 6 animals per group), with osteoclast counts averaged across 3 non-overlapping high-magnification fields per section per animal. ***$p < 0.001$.

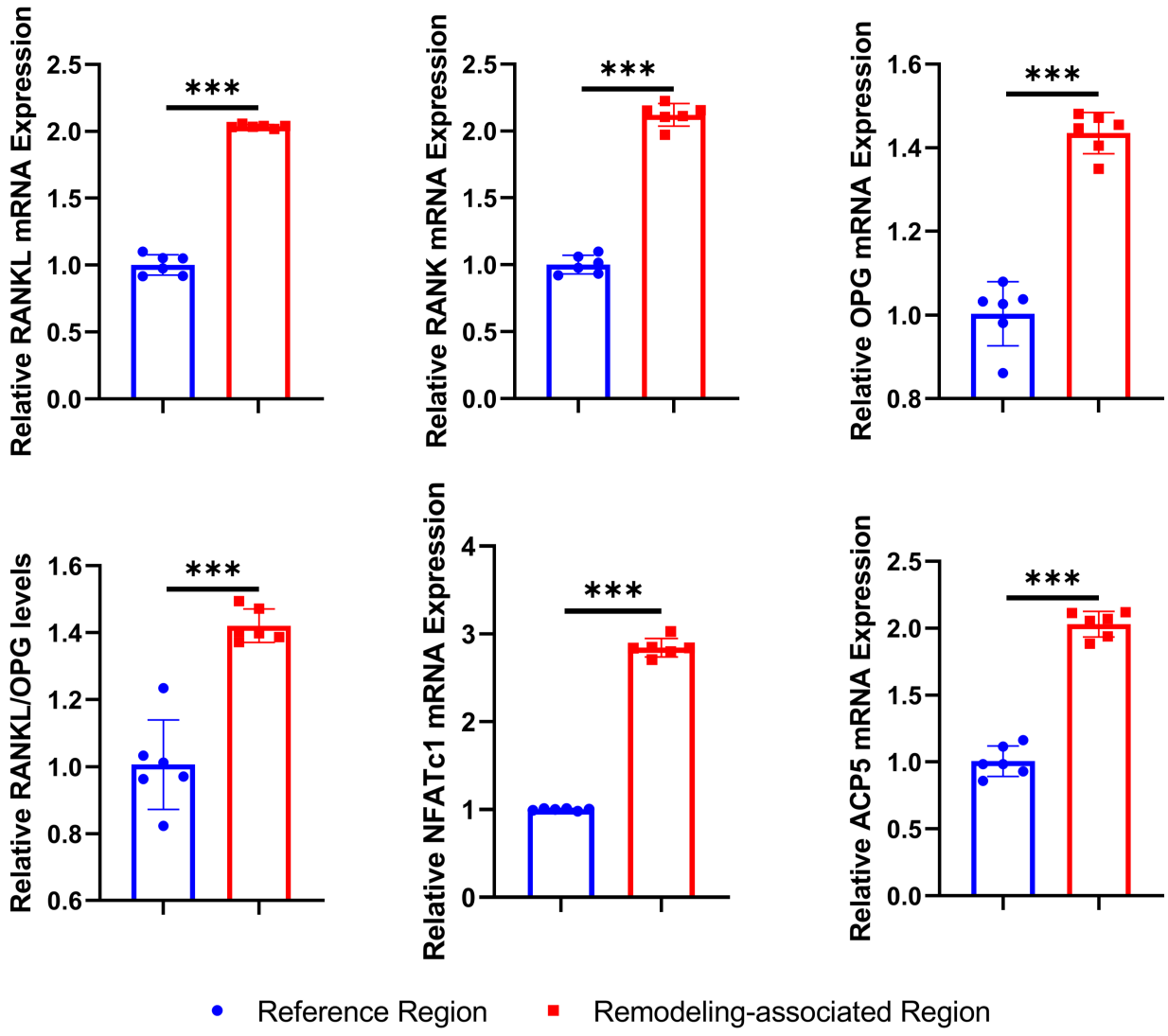

Fig. 3. Gene expression analysis of RANKL/RANK-related molecules in remodeling-associated ROIs isolated by Laser Capture Microdissection (LCM). Quantitative real-time PCR analysis showing mRNA expression levels of RANKL, RANK, OPG, RANKL/OPG ratio, NFATc1, and ACP5. Data were derived from micro-dissected tissues. Gene expression levels were normalized to the internal control and expressed relative to reference tissues. Data are presented as mean ± SD (n = 6 animals, each sample from an independent animal). ***$p < 0.001$.

Discussion

In the present study, we characterized remodeling-associated periodontal regions using a combined histological, spatial, and molecular approach. LCM-based analysis showed increased expression levels of RANKL, RANK, NFATc1, and ACP5, along with an elevated RANKL/OPG ratio in remodeling-associated ROIs. At the tissue level, whole-tissue homogenates also showed increased inflammatory cytokines and osteoclast-related proteins. Complementing the molecular data, immunohistochemical analysis of adjacent serial sections revealed stronger RANKL and RANK immunoreactivity in periodontal regions anatomically corresponding to TRAP-positive osteoclast-enriched areas. Taken together, the LCM-based qPCR data provide the primary evidence for spatially restricted molecular alterations in remodeling-associated periodontal niches, whereas the whole-tissue Western blotting and serial-section immunohistochemistry offer complementary contextual support at the tissue and regional levels, respectively.

A central finding of this investigation is the spatial and quantitative dominance of RANKL over OPG in the remodeling-associated tissues. Under physiological conditions, PDL cells function as a barrier against resorption by constitutively expressing OPG, a decoy receptor that neutralizes RANKL [28]. However, our data suggest that within remodeling-associated microenvironments, the in-

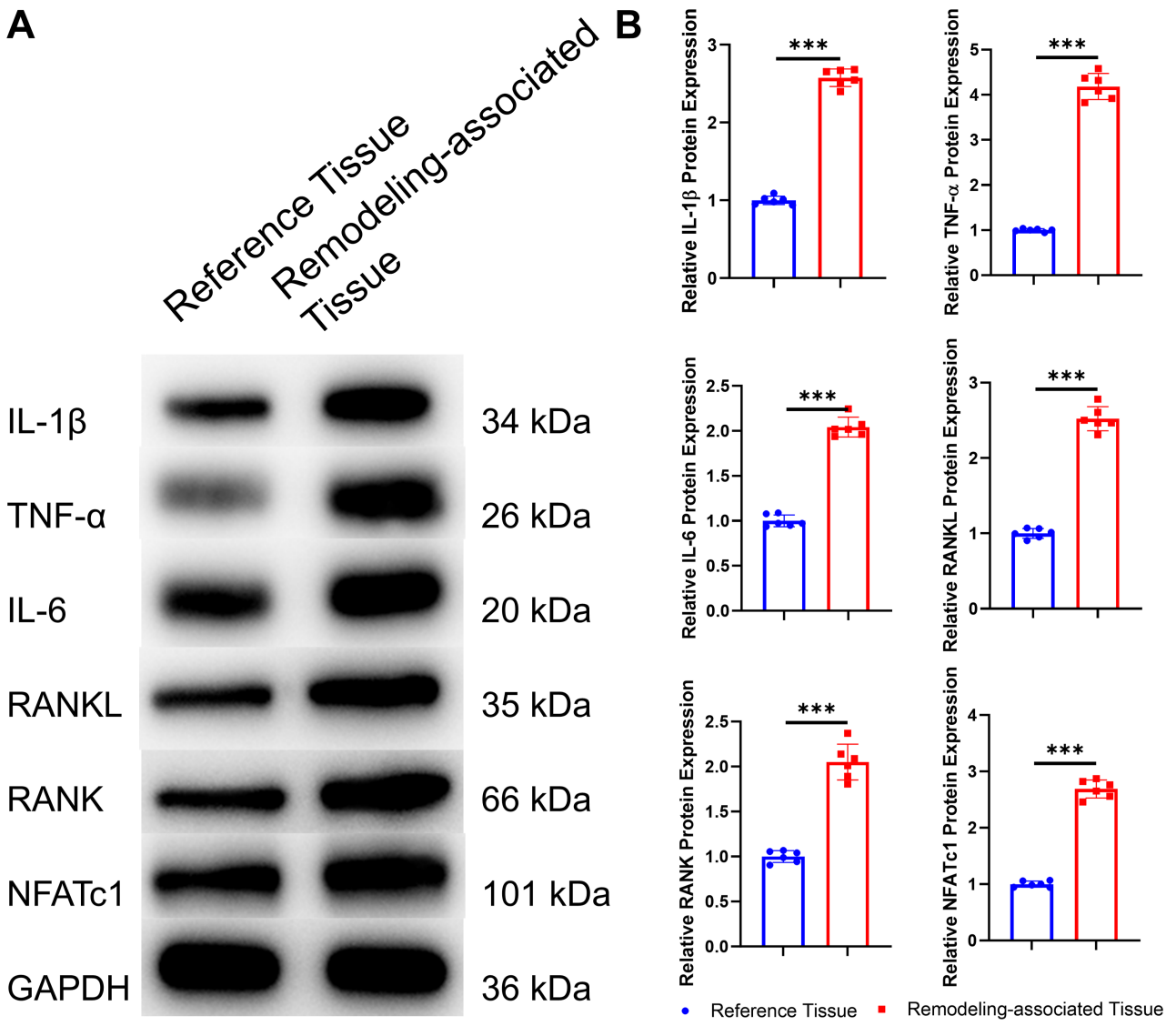

Fig. 4. Inflammatory cytokines and osteoclast-related proteins were elevated in periodontal tissue homogenates. (A) Representative Western blot images showing protein expression of IL-1β, TNF-α, IL-6, RANKL, RANK and NFATc1. Whole-tissue lysates were used for protein analysis to assess the overall inflammatory status. The OTM-loaded maxillary first molar and its contralateral unloaded counterpart from the same animal were used as the experimental and control samples, respectively. (B) Densitometric analysis of corresponding protein expression levels normalized to GAPDH. Protein expression is presented relative to reference tissues. Data are shown as mean ± SD (n = 6 animals per group). ***$p < 0.001$.

crease in RANKL is not matched by a proportional increase in OPG, resulting in a marked elevation of the local RANKL/OPG ratio. While RANKL expression was markedly elevated, OPG levels failed to mount a proportional compensatory response, resulting in a drastically increased RANKL/OPG ratio. This ratio, rather than the absolute concentration of either molecule, serves as a major determinant of osteoclast differentiation potential [29,30]. In adjacent serial sections, stronger RANKL/RANK immunoreactivity was observed in regions corresponding to TRAP-positive osteoclast-enriched areas. This regional correspondence is consistent with the participation of local periodontal cells in remodeling-associated signaling, but the present data do not establish a phenotypic switch at the cellular level.

Downstream of the receptor-ligand interaction, the robust upregulation of NFATc1 observed in the experimental group is consistent with activation of downstream osteoclast-related transcriptional signaling. NFATc1 is widely regarded as the master transcriptional regulator of osteoclastogenesis, responsible for the auto-amplification of its own promoter and the induction of osteoclast-specific genes such as *ACP5* (TRAP) and *Ctsk* [31,32]. It is noteworthy that NFATc1 activation is not solely dependent on

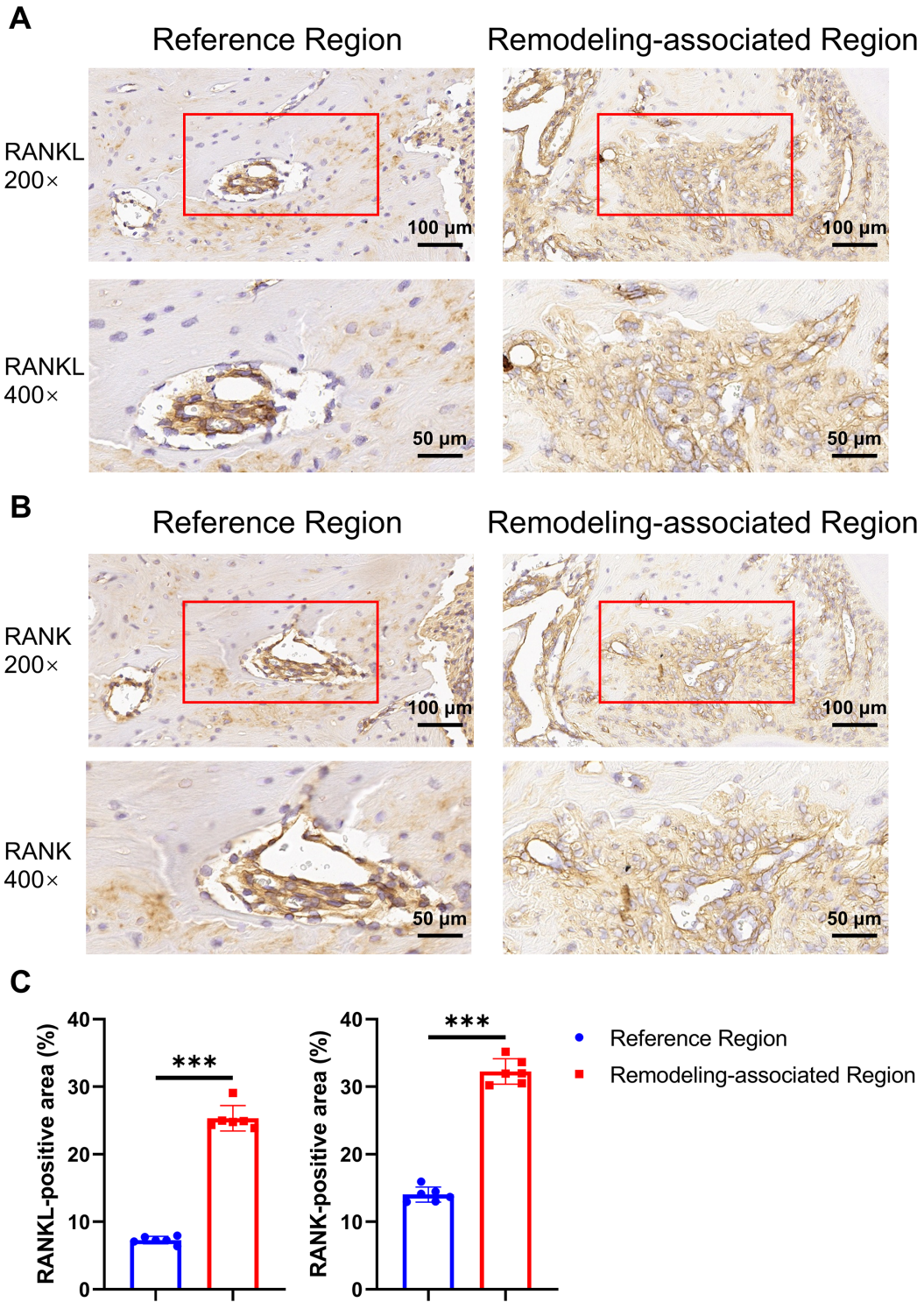

Fig. 5. RANKL and RANK immunoreactivity was observed in anatomically corresponding regions of adjacent serial sections with increased TRAP-positive osteoclasts. (A) Immunohistochemical staining showing RANKL expression predominantly localized within periodontal ligament cells and along alveolar bone surfaces. (B) Immunohistochemical staining demonstrating the distribution of RANK with a similar spatial pattern. (C) Semi-quantitative analysis of RANKL and RANK immunoreactivity expressed as integrated optical density (IOD)/area. Representative images were obtained from anatomically corresponding regions of adjacent serial sections for comparison with TRAP-stained sections in Fig. 2. Data are presented as mean ± SD (n = 6 animals, fields averaged per animal). ***$p <$ 0.001.

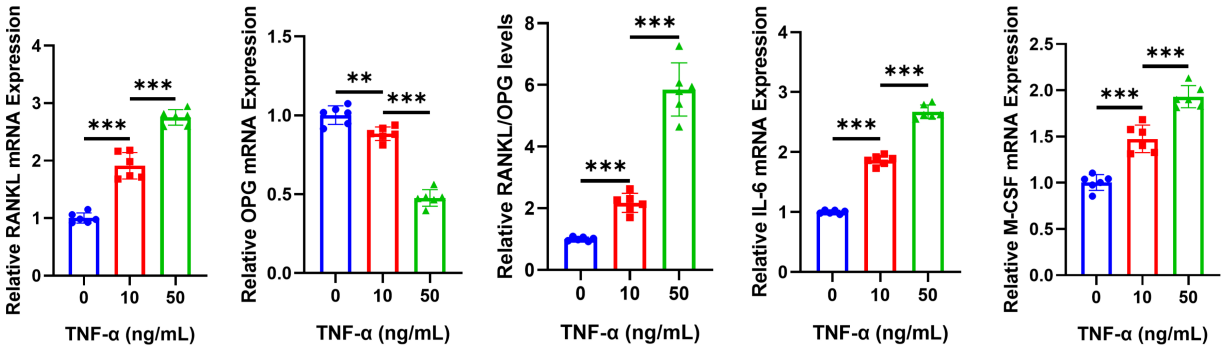

Fig. 6. TNF-α stimulation altered the expression of osteoclast-related and inflammatory markers in hPDLCs. hPDLCs were stimulated with increasing concentrations of TNF-α (0, 10, and 50 ng/mL) for 24 hours to mimic the inflammatory microenvironment. Quantitative real-time PCR analysis of RANKL, OPG, RANKL/OPG ratio, IL-6, and M-CSF mRNA expression. Data are presented as mean ± SD (n = 6 independent experiments). $^{**}p < 0.01$, $^{***}p < 0.001$.

RANKL; inflammatory cytokines, particularly TNF-α and IL-1β, can synergize with RANKL signaling to enhance NFATc1 nuclear translocation and stability [33,34,35]. Our Western blot results showed concomitant increases in inflammatory cytokines and osteoclast-related proteins at the tissue level. Because these measurements were obtained from whole-tissue homogenates, they should be interpreted as tissue-level associations rather than direct evidence of local mechanistic coupling.

We selected TNF-α as the representative inflammatory stimulus. TNF-α occupies an upstream position in the periodontal inflammatory cascade and can induce both IL-1β and IL-6 production in periodontal ligament and stromal cells, allowing it to recapitulate, at least in part, the broader cytokine response [18]. Among the three cytokines, TNF-α has the most direct and best-characterized effect on the RANKL/RANK/OPG axis, the central pathway of the present study, including upregulation of RANKL and modulation of OPG in osteoblastic/stromal lineage cells [11,36]. Also, TNF-α has been repeatedly shown to drive RANKL expression and osteoclastogenic signaling in orthodontic tooth movement models *in vivo* [18,29,37], making it the most representative single-cytokine stimulus for cross-study comparability. The *in vitro* findings provide complementary cellular-level evidence to the *in vivo* spatial data. TNF-α stimulation of hPDLCs dose-dependently increased the *RANKL/OPG* ratio and *M-CSF* expression, suggesting that PDL cells exposed to an inflammatory microenvironment may acquire a molecular profile permissive for osteoclast-related signaling. M-CSF is essential for the survival and proliferation of macrophage/monocyte-lineage osteoclast precursors [38,39]. Given that PDL cells are known to support osteoclast precursor recruitment through paracrine signaling, the concomitant upregulation of M-CSF alongside an elevated *RANKL/OPG* ratio suggests that TNF-α stimulation may increase the expression of molecular cues relevant to both osteoclast precursor support and RANKL-dependent osteoclastogenic signaling within the PDL cell niche. Taken together with the *in vivo* findings demonstrating elevated RANKL, disrupted RANKL/OPG balance, and increased NFATc1 expression within remodeling-associated ROIs, these *in vitro* data suggest a plausible cellular mechanism through which local inflammatory cues may contribute to the altered molecular environment observed in remodeling periodontal niches. Nevertheless, direct evidence linking cytokine-mediated PDL cell responses to osteoclast activation *in vivo* remains to be established in future studies.

From a translational perspective, the present findings suggest that spatially localized inflammatory states may be relevant to periodontal remodeling. However, further mechanistic and interventional studies are needed before any therapeutic implications can be drawn.

A significant strength of this study is the utilization of LCM [40]. Previous studies relying on whole-tissue homogenates often averaged out biological variability, potentially masking the subtle molecular changes occurring specifically at the bone-PDL interface [40,41]. By physically isolating remodeling sites from quiescent tissues, our findings provide a more accurate representation of the local imbalance in the RANKL/OPG ratio associated with osteoclastogenic activity.

Notably, the increase in RANK and RANKL protein levels (Fig. 4) appeared more pronounced than the corresponding mRNA fold changes (Fig. 3). This apparent discrepancy reflects the complementary design of the two assays. Laser-microdissection-based qPCR compared the Remodeling-associated ROI with an adjacent Reference ROI on the same orthodontically loaded tooth, thereby capturing local spatial heterogeneity within the loaded periodontium. Western blotting, performed on whole-tissue lysates, compared the orthodontically loaded tooth with the contralateral unloaded tooth of the same animal, which served as a true physiological baseline. The contralateral baseline is inherently lower than the adjacent Reference ROI on the loaded tooth, and the latter may itself be subject

to systemic or regional contributions of the loaded environment. So, the fold changes obtained by Western blotting are calculated against a lower reference and accordingly amplified. The two readouts thus converge on the same biological conclusion through orthogonal comparisons. Specifically, local intra-tooth heterogeneity was observed at the transcript level, whereas global tissue-level upregulation was reflected at the protein level. Additional contributors include the well-established non-linearity between transcript and protein abundance for RANK/RANKL, owing to translational regulation, protein stability, and membrane retention, as well as the longer integration window of protein accumulation over the 7-day loading period compared with the transient nature of mRNA expression.

Several limitations should be acknowledged. Although comparison of adjacent serial sections allowed assessment of regional correspondence between TRAP-positive osteoclast-rich areas and RANKL/RANK immunoreactivity, the present design did not include double-label staining and therefore cannot establish direct colocalization at the cellular level. Protein expression was assessed using whole-tissue homogenates, which do not provide spatial resolution comparable to that of the LCM-based mRNA analysis. Moreover, TNF-α stimulation of hPDLCs provides supportive evidence that inflammatory stimulation may alter osteoclast-related molecular markers, but does not establish a direct causal relationship between inflammatory cytokines and osteoclast activation in periodontal tissues *in vivo*. We acknowledge that IL-1β and IL-6 are also potent regulators of osteoclast-related signaling, and a direct comparison of the three cytokines, alone and in combination, will be addressed in future studies. In addition, RNA extracted from formalin-fixed, decalcified, and paraffin-embedded periodontal specimens is inevitably fragmented, which can in principle reduce qPCR sensitivity and dynamic range [42]. To mitigate this, we used a standard LCM-FFPE workflow on PEN membrane slides with an FFPE-compatible RNA extraction protocol. We also adopted qPCR primer sets producing short amplicons (~100–150 bp) that are well tolerated by degraded RNA templates, and a strictly within-section design in which Remodeling-associated and Reference ROIs were laser-microdissected from the same tissue section of the same tooth and therefore identically fixed and decalcified. Because both ROIs are affected by RNA fragmentation to a comparable degree, the resulting Ct shifts are largely cancelled by ΔΔCt normalization to GAPDH, allowing reliable relative quantification of transcript abundance between the two regions, as previously demonstrated for FFPE-derived RNA [39]. Nevertheless, absolute transcript quantification remains less robust than that from fresh-frozen material, and future studies using fresh-frozen LCM or paired RNA sequencing are warranted to validate and extend the present findings.

Conclusion

In conclusion, the present study characterized remodeling-associated periodontal microenvironments using a spatially resolved molecular approach. LCM-based analysis demonstrated that disruption of the local RANKL/OPG balance and upregulation of osteoclast-related molecules are spatially restricted features of remodeling niches, rather than uniformly distributed changes across the tissue. Regional correspondence between RANKL/RANK immunoreactivity and TRAP-positive osteoclast-enriched areas, observed in adjacent serial sections, further supports the spatial specificity of these molecular alterations. At the cellular level, TNF-α stimulation of hPDLCs shifted the molecular profile toward a state permissive for osteoclast-related signaling, providing supportive evidence for the *in vivo* observations. Collectively, these findings highlight the importance of spatial resolution in studying periodontal remodeling and suggest that local inflammatory cues may contribute to shaping the osteoclast-related molecular microenvironment within specific remodeling niches. Future investigations incorporating multiplex immunofluorescence or single-cell transcriptomic approaches would allow direct assessment of the cellular colocalization of RANKL/RANK expression with osteoclast activity, whereas *in vivo* conditional knockout or cytokine neutralization models are needed to establish the causal role of inflammatory signaling in periodontal bone remodeling.

Availability of Data and Materials

The data that support the findings of this study are available from the corresponding author upon reasonable request.

Author Contributions

WLL and XPW designed the research study. WLL, CL and JPX performed the research. JZ and XPW analyzed the data. WLL and XPW drafted this article. All authors contributed to important editorial changes in the manuscript. All authors read and approved the final manuscript. All authors have participated sufficiently in the work and agreed to be accountable for all aspects of the work.

Ethics Approval and Consent to Participate

All animal experiments were approved by the Institutional Animal Care and Use Committee of Hebei North University, under protocol number HBNU20251112169, and were conducted in accordance with the ARRIVE Guidelines 2.0.

Acknowledgment

Not applicable.

Funding

This work was supported by 2026 Government-Sponsored Training Project for Outstanding Clinical Medicine Talents, Department of Finance of Hebei Province & Hebei Provincial Health Commission (No. ZF2026340).

Conflict of Interest

The authors declare no conflict of interest.

References

[1] Shi J, Liu Z, Xie J, Zhao Z, Huang X, Cao Z. Engineered extracellular vesicles as multifunctional therapeutics for restoring periodontal homeostasis. Acta Biomaterialia. 2026; 210: 457–480. https://doi.org/10.1016/j.actbio.2025.11.060

[2] Banoriya GK, Singh VK, Maurya R, Kharwar RK. Neuro-Immuno-Endocrine Regulation of Bone Homeostasis. Discovery Medicine. 2025; 37: 464–485. https://doi.org/10.24976/Discov.Med.202537194.39

[3] Hu K, Shang Z, Yang X, Zhang Y, Cao L. Macrophage Polarization and the Regulation of Bone Immunity in Bone Homeostasis. Journal of Inflammation Research. 2023; 16: 3563–3580. https://doi.org/10.2147/JIR.S423819

[4] Tini A, Kumar S, Arasu P, Munusamy N, Balamurugan B, Antony A. Influence of vitamin D in orthodontic tooth movement-a systematic review and meta-analysis of randomized controlled trials in humans. European Journal of Orthodontics. 2024; 46: cjae043. https://doi.org/10.1093/ejo/cjae043

[5] Chen L, Su Y, Wang C, Huang Q, Chen W, Hai N, et al. Rc3h1 negatively regulates osteoclastogenesis by limiting energy metabolism. Theranostics. 2024; 14: 7554–7568. https://doi.org/10.7150/thno.99565

[6] Anuj A, Reuven N, Roberts SGE, Elson A. BASP1 down-regulates RANKL-induced osteoclastogenesis. Experimental Cell Research. 2023; 431: 113758. https://doi.org/10.1016/j.yexcr.2023.113758

[7] Bae S, Kim K, Kang K, Kim H, Lee M, Oh B, et al. RANKL-responsive epigenetic mechanism reprograms macrophages into bone-resorbing osteoclasts. Cellular & Molecular Immunology. 2023; 20: 94–109. https://doi.org/10.1038/s41423-022-00959-x

[8] Xu H, Jia Y, Li J, Huang X, Jiang L, Xiang T, et al. Niloticin inhibits osteoclastogenesis by blocking RANKL-RANK interaction and suppressing the AKT, MAPK, and NF-κB signaling pathways. Biomedicine & Pharmacotherapy = Biomedecine & Pharmacotherapie. 2022; 149: 112902. https://doi.org/10.1016/j.biopha.2022.112902

[9] Zhong Z, Zhang C, Ni S, Ma M, Zhang X, Sang W, et al. NFATc1-mediated expression of SLC7A11 drives sensitivity to TXNRD1 inhibitors in osteoclast precursors. Redox Biology. 2023; 63: 102711. https://doi.org/10.1016/j.redox.2023.102711

[10] Omata Y, Tachibana H, Aizaki Y, Mimura T, Sato K. Essentiality of Nfatc1 short isoform in osteoclast differentiation and its self-regulation. Scientific Reports. 2023; 13: 18797. https://doi.org/10.1038/s41598-023-45909-3

[11] Saidenberg Kermanac'h N, Bessis N, Cohen-Solal M, De Vernejoul MC, Boissier MC. Osteoprotegerin and inflammation. European Cytokine Network. 2002; 13: 144–153.

[12] Zhang Y, Liang J, Liu P, Wang Q, Liu L, Zhao H. The RANK/RANKL/OPG system and tumor bone metastasis: Potential mechanisms and therapeutic strategies. Frontiers in Endocrinology. 2022; 13: 1063815. https://doi.org/10.3389/fendo.2022.1063815

[13] Kim JM, Lin C, Stavre Z, Greenblatt MB, Shim JH. Osteoblast-Osteoclast Communication and Bone Homeostasis. Cells. 2020; 9: 2073. https://doi.org/10.3390/cells9092073

[14] El-Masri BM, Andreasen CM, Laursen KS, Kofod VB, Dahl XG, Nielsen MH, et al. Mapping RANKL- and OPG-expressing cells in bone tissue: the bone surface cells as activators of osteoclastogenesis and promoters of the denosumab rebound effect. Bone Research. 2024; 12: 62. https://doi.org/10.1038/s41413-024-00362-4

[15] Lu J, Shi X, Fu Q, Han Y, Zhu L, Zhou Z, et al. New mechanistic understanding of osteoclast differentiation and bone resorption mediated by P2X7 receptors and PI3K-Akt-GSK3β signaling. Cellular & Molecular Biology Letters. 2024; 29: 100. https://doi.org/10.1186/s11658-024-00614-5

[16] Elson A, Anuj A, Barnea-Zohar M, Reuven N. The origins and formation of bone-resorbing osteoclasts. Bone. 2022; 164: 116538. https://doi.org/10.1016/j.bone.2022.116538

[17] Okamoto K, Takayanagi H. Osteoimmunology. Cold Spring Harbor Perspectives in Medicine. 2019; 9: a031245. https://doi.org/10.1101/cshperspect.a031245

[18] Alghamdi B, Jeon HH, Ni J, Qiu D, Liu A, Hong JJ, et al. Osteoimmunology in Periodontitis and Orthodontic Tooth Movement. Current Osteoporosis Reports. 2023; 21: 128–146. https://doi.org/10.1007/s11914-023-00774-x

[19] Bousch JF, Beyersdorf C, Schultz K, Windolf J, Suschek CV, Maus U. Proinflammatory Cytokines Enhance the Mineralization, Proliferation, and Metabolic Activity of Primary Human Osteoblast-like Cells. International Journal of Molecular Sciences. 2024; 25: 12358. https://doi.org/10.3390/ijms252212358

[20] Li Y, Huang Z, Pan S, Feng Y, He H, Cheng S, et al. Resveratrol Alleviates Diabetic Periodontitis-Induced Alveolar Osteocyte Ferroptosis Possibly via Regulation of SLC7A11/GPX4. Nutrients. 2023; 15: 2115. https://doi.org/10.3390/nu15092115

[21] Yamada C, Ho A, Garcia C, Oblak AL, Bissel S, Porosencova T, et al. Dementia exacerbates periodontal bone loss in females. Journal of Periodontal Research. 2024; 59: 512–520. https://doi.org/10.1111/jre.13227

[22] Petrović A, Trandafilović M, Drevenšek G, Plut A, Drevenšek M. Periodontal ligament regulatory role in experimental diabetic rat model of periodontium remodelling. Folia Morphologica. 2022; 81: 1031–1041. https://doi.org/10.5603/FM.a2021.0101

[23] Arai C, Nomura Y, Ishikawa M, Noda K, Choi JW, Yashiro Y, et al. HSPA1A is upregulated in periodontal ligament at early stage of tooth movement in rats. Histochemistry and Cell Biology. 2010; 134: 337–343. https://doi.org/10.1007/s00418-010-0737-3

[24] Marcantonio CC, Lopes MES, Soares LFF, Salmon CR, Nociti Junior FH, Deschner J, et al. Proteomic Analysis of the Periodontal Ligament During Orthodontic Movement: A Study in Rats. Proteomes. 2025; 13: 42. https://doi.org/10.3390/proteomes13030042

[25] Yongchaitrakul T, Lertsirirangson K, Pavasant P. Human periodontal ligament cells secrete macrophage colony-stimulating factor in response to tumor necrosis factor-alpha in vitro. Journal of Periodontology. 2006; 77: 955–962. https://doi.org/10.1902/jop.2006.050338

[26] Heo SC, Kim YN, Choi Y, Joo JY, Hwang JJ, Bae MK, et al. Elevated Expression of Cathepsin K in Periodontal Ligament Fibroblast by Inflammatory Cytokines Accelerates Osteoclastogenesis via Paracrine Mechanism in Periodontal Disease. Inter-

national Journal of Molecular Sciences. 2021; 22: 695. https://doi.org/10.3390/ijms22020695

[27] Knaup I, Kramann R, Sasula MJ, Mack P, Bastos Craveiro R, Niederau C, et al. TNF reduces osteogenic cell fate in PDL cells at transcriptional and functional levels without alteration of periodontal proliferative capacity. Journal of Orofacial Orthopedics = Fortschritte Der Kieferorthopadie : Organ/official Journal Deutsche Gesellschaft Fur Kieferorthopadie. 2025; 86: 12–21. https://doi.org/10.1007/s00056-024-00541-2

[28] Santos BZD, Dutra RC, Santos ARSD, Casarin M, Goldfeder EM, Bosco VL, et al. Immunohistochemistry of resorption and inflammation factors in the periodontal ligament of human deciduous teeth. Brazilian Oral Research. 2022; 36: e056. https://doi.org/10.1590/1807-3107bor-2022.vol36.0056

[29] Tan K, Wang J, Su X, Zheng Y, Li W. KAT6A/YAP/TEAD4 pathway modulates osteoclastogenesis by regulating the RANKL/OPG ratio on the compression side during orthodontic tooth movement. Progress in Orthodontics. 2024; 25: 29. https://doi.org/10.1186/s40510-024-00530-6

[30] Uchinuma M, Taketani Y, Kanaya R, Yamane Y, Shiota K, Suzuki R, et al. Role of Piezo1 in modulating the RANKL/OPG ratio in mouse osteoblast cells exposed to Porphyromonas gingivalis lipopolysaccharide and mechanical stress. Journal of Periodontal Research. 2024; 59: 749–757. https://doi.org/10.1111/jre.13265

[31] Zhu M, Xu M, Bertheloot D, Brom VC, Sieberath A, Salber J, et al. Arcyriaflavin A Alleviates Osteoporosis by Suppressing RANKL-Induced Osteoclastogenesis. International Journal of Molecular Sciences. 2025; 26: 2141. https://doi.org/10.3390/ijms26052141

[32] Li H, Deng W, Yang J, Lin Y, Zhang S, Liang Z, et al. Corylifol A suppresses osteoclastogenesis and alleviates ovariectomy-induced bone loss via attenuating ROS production and impairing mitochondrial function. Biomedicine & Pharmacotherapy = Biomedecine & Pharmacotherapie. 2024; 171: 116166. https://doi.org/10.1016/j.biopha.2024.116166

[33] Lu F, Wu X, Hu H, Zhang J, Song X, Jin X, et al. Yangonin treats inflammatory osteoporosis by inhibiting the secretion of inflammatory factors and RANKL expression. Inflammopharmacology. 2022; 30: 1445–1458. https://doi.org/10.1007/s10787-022-00985-1

[34] Wang X, Sun L, An Z, Li C, Zhao J. CXCL7 enhances RANKL-induced osteoclastogenesis via the activation of ERK/NFATc1 signaling pathway in inflammatory arthritis. Arthritis Research & Therapy. 2025; 27: 34. https://doi.org/10.1186/s13075-025-03502-1

[35] Liu C, Zuo M, Zhao J, Niu T, Hu A, Wang H, et al. DPHB inhibits osteoclastogenesis by suppressing NF-κB and MAPK signaling and alleviates inflammatory bone destruction. International Immunopharmacology. 2025; 152: 114377. https://doi.org/10.1016/j.intimp.2025.114377

[36] Hofbauer LC, Lacey DL, Dunstan CR, Spelsberg TC, Riggs BL, Khosla S. Interleukin-1beta and tumor necrosis factor-alpha, but not interleukin-6, stimulate osteoprotegerin ligand gene expression in human osteoblastic cells. Bone. 1999; 25: 255–259. https://doi.org/10.1016/s8756-3282(99)00162-3

[37] Marahleh A, Kitaura H, Ohori F, Noguchi T, Nara Y, Pramusita A, et al. Effect of TNF-α on osteocyte RANKL expression during orthodontic tooth movement. Journal of Dental Sciences. 2021; 16: 1191–1197. https://doi.org/10.1016/j.jds.2021.03.006

[38] Ibáñez L, Nácher-Juan J, Terencio MC, Ferrándiz ML, Alcaraz MJ. Osteostatin Inhibits M-CSF+RANKL-Induced Human Osteoclast Differentiation by Modulating NFATc1. International Journal of Molecular Sciences. 2022; 23: 8551. https://doi.org/10.3390/ijms23158551

[39] Starlinger J, Sarahrudi K, Kecht M, Koerbler F, Pietschmann P, Aharinejad S. The influence of M-CSF on fracture healing in a mouse model. Scientific Reports. 2021; 11: 22326. https://doi.org/10.1038/s41598-021-01673-w

[40] Guo W, Hu Y, Qian J, Zhu L, Cheng J, Liao J, et al. Laser capture microdissection for biomedical research: towards high-throughput, multi-omics, and single-cell resolution. Journal of Genetics and Genomics = Yi Chuan Xue Bao. 2023; 50: 641–651. https://doi.org/10.1016/j.jgg.2023.07.011

[41] Nogueira M, Golbert DCF, Landeira B, Leão RN. Laser Capture Microdissection Optimization for High-Quality RNA in Mouse Brain Tissue. Current Protocols. 2022; 2: e457. https://doi.org/10.1002/cpz1.457

[42] Antonov J, Goldstein DR, Oberli A, Baltzer A, Pirotta M, Fleischmann A, et al. Reliable gene expression measurements from degraded RNA by quantitative real-time PCR depend on short amplicons and a proper normalization. Laboratory Investigation; a Journal of Technical Methods and Pathology. 2005; 85: 1040–1050. https://doi.org/10.1038/labinvest.3700303